Tilted anisotropic Dirac cones in partially hydrogenated graphene

Hong-Yan Lu,[1,2,*] Armindo S. Cuamba,[1] Shih-Yang Lin,[1,3] Lei Hao,[1,4] Rui Wang,[1,5] Hai Li,[1] YuanYuan Zhao,[1] and C. S. Ting[1]

[1]*Texas Center for Superconductivity and Department of Physics, University of Houston, Houston, Texas 77204, USA*

[2]*School of Physics and Electronic Information, Huaibei Normal University, Huaibei 235000, China*

[3]*Department of Physics, National Cheng Kung University, Tainan 701, Taiwan*

[4]*Department of Physics, Southeast University, Nanjing 210096, China*

[5]*National Laboratory of Solid State Microstructures and Department of Physics, Nanjing University, Nanjing 210093, China*

(Received 24 May 2016; revised manuscript received 27 October 2016; published 15 November 2016)

By means of first-principles calculations, we predict a partially hydrogenated graphene system, C_6H_2, and find the one in AB-trans configuration is a Dirac material with a tilted anisotropic Dirac cone electronic structure. Different from graphene, in which the Dirac points are located at K and K' and the Fermi surfaces are circular with doping, the AB-trans C_6H_2 exhibits Dirac points located on the lines from Γ to M with quasielliptical Fermi surfaces when doped. Around the Dirac point, the Fermi velocity varies along different directions. Therefore, the propagation of charge carriers in this system is highly anisotropic, creating a new tunability for novel transport properties.

DOI: 10.1103/PhysRevB.94.195423

I. INTRODUCTION

Dirac materials, in which the low-energy electrons obey the relativistic Dirac equation, have attracted a lot of attention in past years [1,2]. The most studied Dirac material is graphene with the massless Dirac cones near the zone corners [3,4]. Recently, more and more Dirac materials have been reported, for example, topological insulators with their characteristic Dirac cones in the surface state [5,6], the parent compound of iron-based superconductor in the collinear magnetic state [7], three-dimensional Dirac semimetals [8–12], and two-dimensional silicene [13,14], with the list growing rapidly. Many intriguing properties of Dirac materials have been investigated, such as ultrahigh carrier mobility [15], unconventional quantum Hall effect, Klein tunneling, etc. [2,4].

In addition to searching for new Dirac materials, generating Dirac cone anisotropy has also attracted much attention. It is proved that the conductance for anisotropic cones varies strongly with transport direction [16], which can be used for designing new electronic devices. Until now, several systems have been found with anisotropic Dirac cone band structure. For example, VO_2-TiO_2 nanoheterostructures [17,18], AMnBi$_2$ (A = Sr or Ca) [19–21], topological insulators β-Ag_2Te, β-HgS, HgSe, and HgTe [22,23], as well as doped few-layer black phosphorus [24]. Besides, two-dimensional carbon allotropes, such as certain graphynes [25–27], rectangular graphene [28] and phagraphene [29] exhibit anisotropic Dirac cones, too. Due to its natural Dirac cone structure, graphene also serves as an important platform to support anisotropic Dirac transport with proper manipulations, for example, by applying periodic potentials [30] or uniaxial strain [31]. While the above realizations rely on external driving and may bring more challenges in experimental conditions, the question arises whether one could create intrinsic anisotropic Dirac materials in graphene systems that do not need external modulation.

In recent years, hydrogenation of graphene has attracted increasing interest because it can modify the electronic properties of graphene, providing a possible way for functioning it to show specially desired features. The hydrogenation of graphene is reversible [32], providing the flexibility to manipulate the coverage of hydrogen. For instance, fully hydrogenated graphene, called graphane, with hydrogen atoms bonded to carbon atoms alternatively on both sides of the graphene plane, was theoretically predicted [33] and experimentally synthesized [32]. It is a semiconductor with a direct band gap of 3.5 eV. Later, semihydrogenated graphene, called graphone, with the hydrogen atoms on one side of graphane removed, was theoretically predicted to be a ferromagnetic (FM) semiconductor with an indirect gap of 0.46 eV [34]. Moreover, the stable two-dimensional C_4H with periodic structure was experimentally synthesized, which is a semiconductor with an indirect gap of 3.5 eV [35]. Besides, there are several works studying the electronic properties of graphene with various hydrogen distributions and concentrations [36–47], it is found that the electronic properties of graphene can be altered dramatically, e.g., the opening of a band gap, tuning the magnitude of the band gap of hydrogenated graphene by hydrogen coverage, etc. However, whether Dirac material with anisotropic Dirac cones can be obtained by hydrogenating graphene is still an open question.

Based on the above concerns and first-principles calculations, in this work, we propose a hydrogenated graphene system: C_6H_2. Interestingly, we find that the one in AB-trans configuration is a Dirac material with a tilted anisotropic Dirac cone. Unlike graphene, in which the positions of the Dirac points are located at K and K' and the Fermi surfaces (FSs) are circular when doped, it is found that the Dirac points for AB-trans C_6H_2 are located on the lines from Γ to M and the Fermi surfaces are quasielliptical with doping. Around the Dirac point, the Fermi velocity varies along different directions. Consequently, the propagation of charge carriers in this system is highly anisotropic, creating a new tunability for novel transport properties.

II. COMPUTATIONAL DETAILS

The calculations of C_6H_2 are performed within density functional theory (DFT) as implemented in the QUANTUM

*luhongyan2006@gmail.com

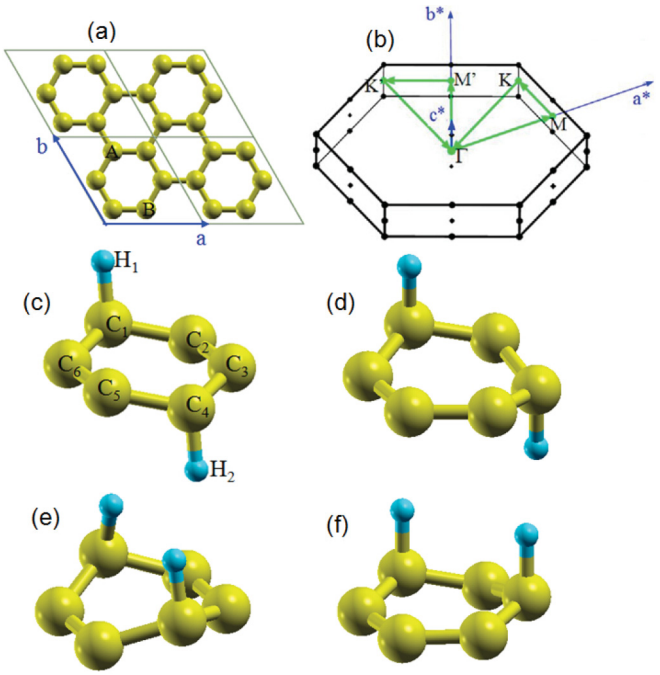

FIG. 1. (a) Periodic structure with six carbon atoms in a unit cell. C_6H_2 can be obtained by hydrogenating two carbon atoms in a unit cell. The two sublattices are labeled as A and B. (b) First Brillouin zone (BZ) and high-symmetry points for C_6H_2. High-symmetry lines are shown in green color, along which the band structure and phonon spectra will be plotted. (c)–(f) The optimized structures of C_6H_2 unit cell in AB-trans, AA-trans, AB-cis, and AA-cis configurations, respectively. In (c), the atoms are labeled to better describe their contributions.

ESPRESSO (QE) program [48]. We adopt the projector augmented wave method [49] to model the electron-ion interactions, and the generalized gradient approximation (GGA) with Perdew-Burke-Ernzerhof parametrization [50] for the exchange correlation potentials. The lattice dynamics is performed within the framework of the density functional perturbation theory (DFPT) [51] as implemented in QE [48]. We perform a full structural optimization, including both the lattice parameters and the atom positions. The precision for the convergence of total energy and force are 10^{-7} Ry and 10^{-6} Ry/Bohr, respectively. The cutoffs for wave functions and charge density are 80 Ry and 480 Ry, respectively. The electronic integration is performed over a $12 \times 12 \times 1$ k-point mesh. For the FS and density of states (DOS) calculations, denser $48 \times 48 \times 4$ and $150 \times 150 \times 1$ k-point grids are respectively adopted. For the phonon calculation, the dynamical matrices are calculated on a $8 \times 8 \times 1$ q-point grid.

The initial lattice structure of C_6H_2 is based on a graphene lattice. We adopt a periodic structure with six carbon atoms as a unit cell, and the basis vectors are along the armchair directions of carbon atoms, as can be seen in Fig. 1(a). C_6H_2 can be obtained by hydrogenating two carbon atoms in a unit cell. It is well known that there are two sublattices A and B in graphene. In the 6-C unit cell, two hydrogen atoms can bond with two carbon atoms on the same sublattice or on different sublattices, which can be named as AA and AB hydrogenations, respectively. Besides, the two hydrogen atoms can be on the same side or on different sides of the graphene plane, which are called cis and trans configurations, respectively. Therefore, four different configurations for C_6H_2 are expected: AB-trans, AA-trans, AB-cis, and AA-cis. The initial C-C bond length is set as 1.42 Å as in graphene [4], and the C-H bond length is set as 1.11 Å as in graphane [33]. A vacuum space of 20 Å normal to the graphene layer is used to avoid interactions between adjacent layers.

TABLE I. The total energies and formation energies per unit cell for AB-trans, AA-trans, AB-cis, and AA-cis configurations. For the AA-trans and AA-cis cases, the results are for the FM ground state.

Configuration	AB-trans	AA-trans	AB-cis	AA-cis
Total energy (Ry)	–112.933	–112.766	–112.885	–112.759
Formation energy (Ry)	–0.265	–0.098	–0.217	–0.091

III. RESULTS AND DISCUSSION

The optimized structures for C_6H_2 unit cell in AB-trans, AA-trans, AB-cis, and AA-cis configurations are shown in Figs. 1(c)–1(f), respectively. Similar to graphane and graphone, due to the formation of a C-H bond, the hydrogenated carbon atoms are pulled out of the graphene plane. By self-consistent calculation with the spin polarization taken into account, we investigate the magnetic properties for the four cases and find that the AB-trans and AB-cis configurations show nonmagnetic (NM) ground states, whereas the AA-trans and AA-cis configurations show FM ground states with the total/absolute magnetization of about 2 μ_B/cell. Specifically, the total energies for AA-trans and AA-cis configurations in the FM state are respectively 0.008 and 0.02 Ry lower than those in the NM state. Thus, the two AA configurations are in FM ground states. The total energies for the four cases are listed in Table I. It is seen that the AB hydrogenations always show lower energy than the AA hydrogenations, and the AB-trans configuration shows the lowest energy and must be the most energetically favorable case among the four configurations.

To prove the stability of C_6H_2 in the four configurations, two aspects are carefully investigated. First, we calculate the formation energy relative to graphene and hydrogen atoms, as would be typical in the experimental setup [32,35,37,52]. As shown in Table I, the negative formation energies suggest that all the four configurations are thermodynamically stable, with the AB-trans configuration the easiest to be formed. Second, to examine their dynamic stability, we calculate the phonon spectra for the four cases along the high-symmetry line Γ-M-K-Γ-M'-K'-Γ [denoted by green arrows in Fig. 1(b)], with the results shown in Fig. 2. For the AB-trans case, a wide range of frequency extending up to about 2853 cm^{-1} is observed, which is shown in Fig. 2(a). Importantly, no imaginary frequency emerges in the full phonon spectra, justifying its dynamical stability. Particularly, the two highest-frequency modes, occurring respectively at 2830 and 2853 cm^{-1}, correspond to the C-H stretching modes. They are respectively Raman and infrared active, which should be useful for characterizing this compound in experiment. However, for the phonon spectra of AA-trans configuration in Fig. 2(b), the

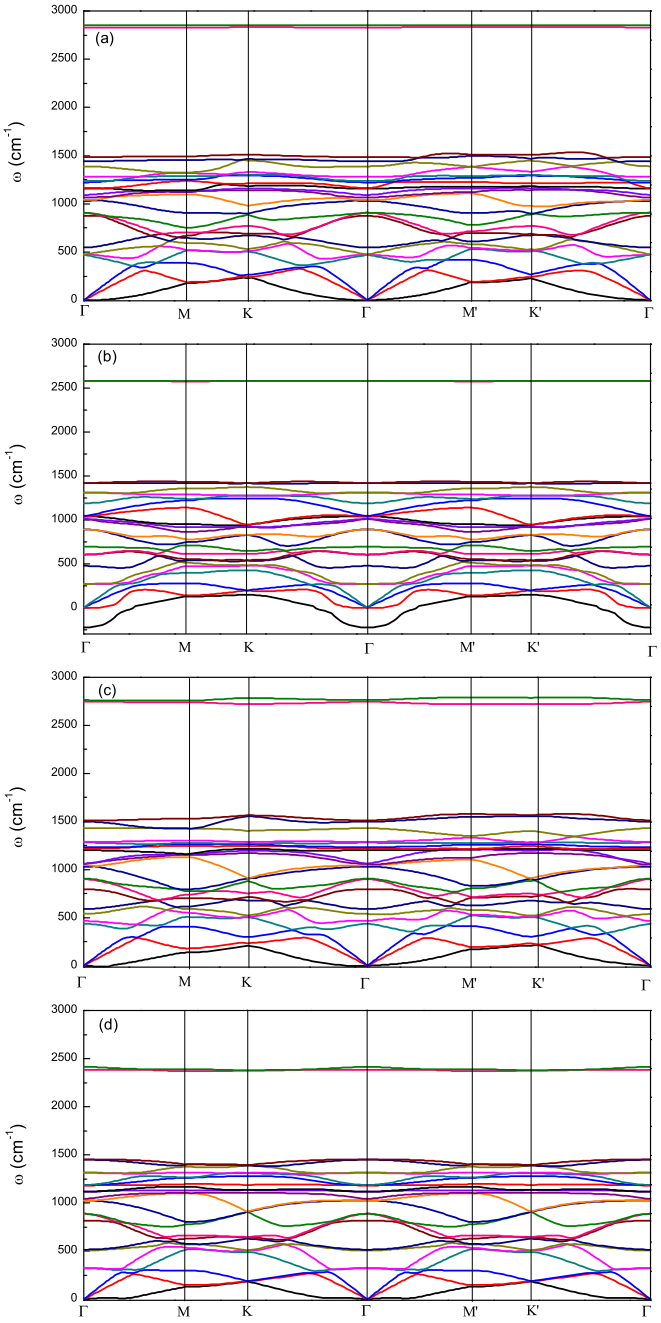

FIG. 2. Phonon spectra of C_6H_2 in (a) AB-trans, (b) AA-trans, (c) AB-cis, and (d) AA-cis configurations.

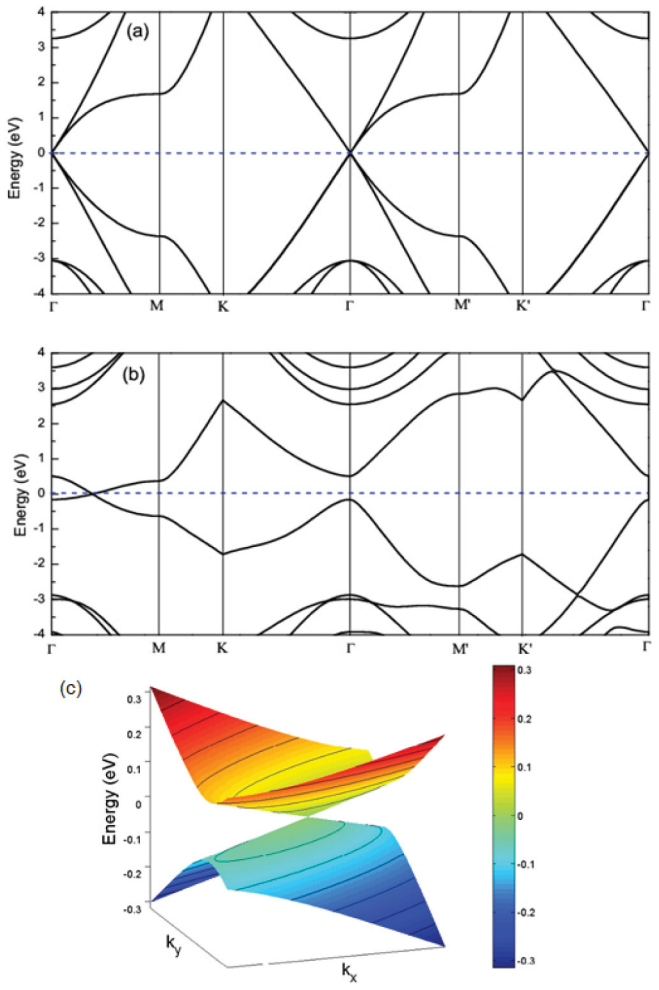

FIG. 3. (a) Electronic band structure of unhydrogenated graphene within the 6-C unit cell [shown in Fig. 1(a)] in the first BZ along the high-symmetry line Γ-M-K-Γ-M'-K'-Γ. (b) Electronic band structure of AB-trans C_6H_2 along the high-symmetry line Γ-M-K-Γ-M'-K'-Γ. (c) Three-dimensional low-energy dispersion around one Dirac point. The contour lines of constant energy are shown in black. The Fermi level is set to be zero in (a), (b), and (c).

lowest branch shows an imaginary frequency at around the Γ point, with the frequency about –226 cm^{-1}, indicating that it is dynamically unstable. For the phonon spectra of the AB-cis and AA-cis configurations respectively shown in Figs. 2(c) and 2(d), there are also no imaginary frequencies in the phonon spectra. However, around the Γ point, the lowest phonon spectrum, which corresponds to an out-of-plane transverse acoustic mode (or ZA mode), is very flat and close to zero along certain directions, indicating that the lattices could be very soft and may not be very stable. On the other hand, we also note that soft modes are very natural in two-dimensional materials, a feature intimately related to the intrinsic tendency for them to develop transverse vibrations. Since the stable AB-trans configuration shows the lowest formation energy, it must be the easiest to be realized. Therefore, in the following calculations, we only concentrate on the AB-trans configuration.

For the optimized lattice structure of AB-trans C_6H_2 in Fig. 1(c), there are four kinds of C-C bonds with different bond lengths. Within a unit cell, the length of the C-C bond with one C bonded with H is 1.51 Å, whereas for the unhydrogenated carbon atoms, the C-C bond length is 1.40 Å. Between nearest-neighboring unit cells, for the bond between two hydrogenated/unhydrogenated C atoms, the C-C bond length is 1.53/1.41 Å. The C-H bond length is the same as that of graphane, i.e., 1.11 Å [33]. Based on the optimized lattice structure, we calculate the electronic structure of AB-trans C_6H_2. For comparison, we first calculate the band structure of unhydrogenated graphene in the reduced Brillouin zone (BZ) within the 6-C unit cell, with the result shown in Fig. 3(a). It is seen that there is a Dirac cone with the Dirac point located at

Γ, which is equivalent to the K and K' points in the 2-C unit cell because of the BZ folding. Besides, the band structure along Γ-M-K-Γ is the same with that along Γ-M'-K'-Γ due to the C_6 rotational symmetry of graphene. While, for AB-trans C_6H_2, as seen in Fig. 1(c), the rotational symmetry is reduced to C_2. This leads to different band structures along the two paths, which can be clearly seen in Fig. 3(b). What is particularly interesting is that there is a Dirac cone with the Dirac point located at an off-symmetry point (0.191, 0.110, 0)$\times 2\pi/a$ between Γ and M (in Cartesian coordinates with a the length of basis for AB-trans C_6H_2 after relaxation), totally different from graphene where the Dirac points are located at K and K' points in the 2-C unit cell. Along M-K-Γ-M'-K'-Γ, the band structure is fully gapped. Moreover, the bands above and below the Fermi level are not symmetric even near the Dirac point, which leads to particle-hole asymmetry.

To be more intuitive, we plot the three-dimensional low-energy dispersion around the Dirac point, which is shown in Fig. 3(c). The valence band and the conduction band intersect with each other at the Fermi level, but the Fermi velocity varies along different directions, leading to the anisotropic Dirac cone electronic structure. The contour lines of constant energy are shown in black, from which we can see that the Dirac cone is tilted along Γ-M direction. It is well known that the Fermi velocity for graphene is 10^6 m/s along all the directions around the Dirac point. For comparison, we calculate the Fermi velocities from the Dirac point along various directions by $v_F = \nabla_k E/\hbar$, where the gradient is taken along a particular direction to get the velocity along that direction. It is found that the result from the Dirac point to M direction differs from that from the Dirac point to Γ direction, i.e., 1.3×10^5 m/s and 3.4×10^5 m/s, respectively, confirming the tilted anisotropic Dirac cone electronic structure. While perpendicular to Γ-M direction, the Fermi velocity is the biggest with the value of 7.6×10^5 m/s. The tilted Dirac cone electronic structure is similar to that of graphene under uniaxial strain [31]. Although the Fermi velocities of AB-trans C_6H_2 are a little smaller than that of graphene, the significant anisotropy creates a new tunability for novel transport properties.

The existence of Dirac cones in the band structure of AB-trans C_6H_2 and their positions can be understood qualitatively as follows. Compared with the pristine graphene, the unit cell of the AB-trans C_6H_2 enlarges three times. If the enlargement of the unit cell is the only change in the lattice of AB-trans C_6H_2 compared with that of the pristine graphene, the BZ of the AB-trans C_6H_2 will be obtained from that of the graphene by folding to 1/3 of the latter. In this process, the Dirac points of graphene will be folded to the Γ point of the BZ for C_6H_2, as shown in Fig. 3(a). In reality, however, the symmetry of AB-trans C_6H_2 lattice also reduces to C_{2h} from the original C_{6h} of graphene. The absence of threefold symmetry indicates that the Dirac points would in general no longer be folded to the Γ point of the new BZ. Suppose one Dirac point is folded to a general point of the BZ, then from the C_{2h} symmetry there should be four Dirac points in the BZ. This is impossible because there are only two Dirac points in the original BZ of graphene. Therefore, the Dirac points, if they exist, must appear along high-symmetry axes. These include Γ-M and Γ-K'. In addition, the degeneracy at the Dirac points are not protected by a fundamental symmetry of the lattice, because the C_{2h} point group has only one-dimensional irreducible representations. Therefore, on the one hand Dirac points can only appear along Γ-M or Γ-K', and on the other hand whether or not they indeed appear depends on specific lattice parameters. What follows are some qualitative behaviors of the Dirac cones inferred from test calculations based on tight-binding model and DFT.

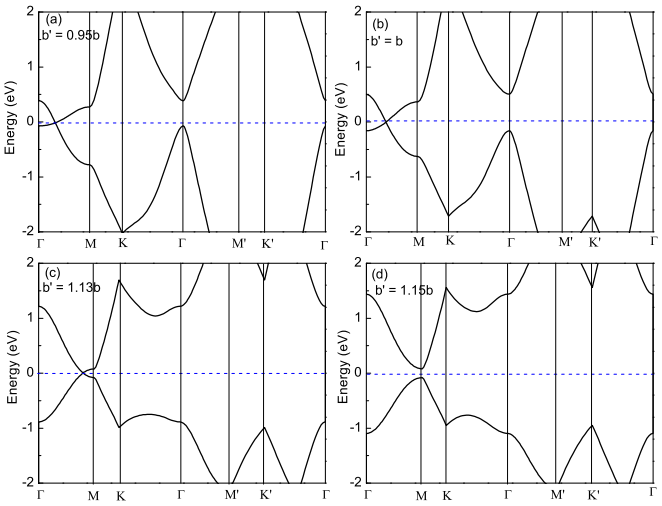

FIG. 4. Band structures for (a) $b' = 0.95b$, (b) $b' = b$, (c) $b' = 1.13b$, and (d) $b' = 1.15b$, with the length of basis a unchanged. Here, a and b are the lengths of lattice basis of AB-trans C_6H_2 after relaxation.

First, from test calculations based on tight-binding model, the reason why the Dirac points are not at the Γ point lies in the presence of two types of C-C bonds which connect unhydrogenated C atoms. Namely, the bond length of the C-C bonds connecting unhydrogenated C atoms in the same unit cell is different from that connecting unhydrogenated C atoms between neighboring unit cells. This leads to the difference in the corresponding hopping integrals. Second, by first-principles calculations, we calculate the band structures by tuning the length of basis b with the length of basis a unchanged. The results for $b' = 0.95b$, b, $1.13b$, and $1.15b$ are shown in Fig. 4. We find that as b is decreased, the Dirac cones become more tilted, while as b is increased, the Dirac cones become less tilted, shift continuously to the M point, and finally disappear. From the above results we can conclude that Dirac points can appear along Γ-M, and the appearance of the Dirac cones depends on specific lattice parameters.

In addition, we calculate the total DOS and orbital-projected DOS for each atom in AB-trans C_6H_2. The results are presented in Fig. 5. From Fig. 5(a), it is seen that the total DOS is zero at the Fermi level, consistent with the Dirac cone band structure. The particle-hole asymmetry can also be seen. It is well known that the DOS around the Fermi level is proportional to the energy |E| for graphene. For AB-trans C_6H_2, similar linear behavior around the Dirac point can be found. To find which atoms contribute most to the electronic states near the Fermi level, we plot the orbital-projected DOS for all the atoms in the unit cell. The results are shown in Fig. 5(b). Before discussing them, we first look at the lattice structure in Fig. 1(c). It is found that the eight atoms in the

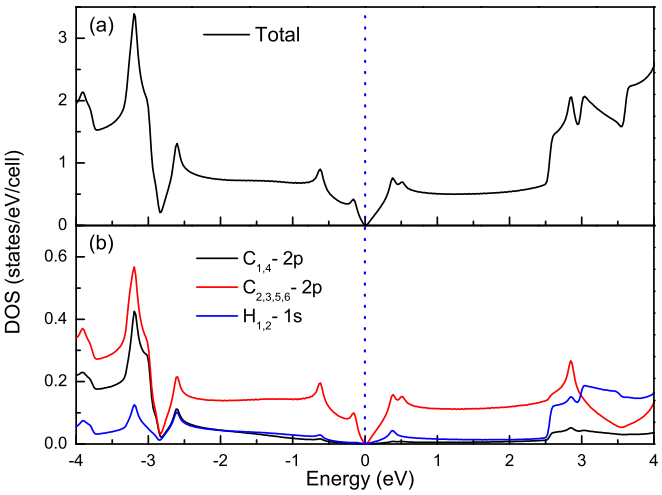

FIG. 5. (a) Total electronic DOS for AB-trans C_6H_2. (b) Orbital-projected electronic DOS for each atom in AB-trans C_6H_2 unit cell.

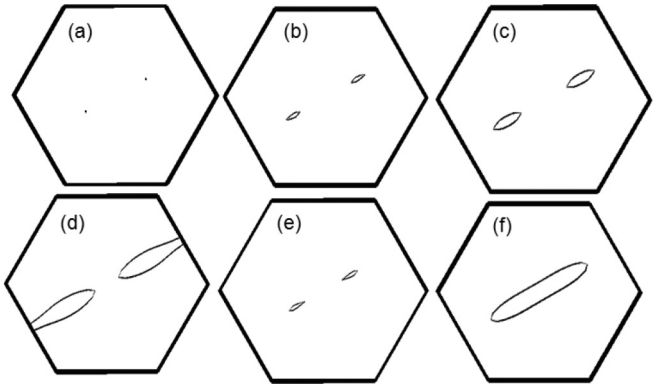

FIG. 6. FSs for undoped (a), electron-doped (b)–(d), and hole-doped (e), (f) cases of AB-trans C_6H_2. For the electron-doped cases, the Fermi level moves 0.1 eV (b), 0.2 eV (c), and 0.4 eV (d) upwards, and for the hole-doped cases, the Fermi level moves –0.1 eV (e), and –0.4 eV (f) downwards relative to the undoped case.

unit cell can be divided into three groups: (1) $C_{1,4}$ atoms, (2) $C_{2,3,5,6}$ atoms, and (3) $H_{1,2}$ atoms, with each group showing the same DOS. The reason is that $C_{1,4}$ atoms are the hydrogenated carbon atoms, $C_{2,3,5,6}$ atoms are the nearest neighbors of hydrogenated carbon atoms, and $H_{1,2}$ atoms are symmetric relative to the center of the unit cell. Therefore, the lattice symmetry determines that the DOS for the atoms in the same group are the same. From Fig. 5(b), we can see that $C_{2,3,5,6}$ atoms, i.e., the unhydrogenated carbon atoms, contribute most to the total DOS near the Fermi level, while $C_{1,4}$ atoms and $H_{1,2}$ atoms contribute little to the DOS around the Fermi level. To be more specific, we check and find that the DOS mainly comes from the $2p_z$ orbital (π electrons) of the $C_{2,3,5,6}$ atoms. This can be understood by the fact that the $C_{1,4}$ atoms form strong σ bonds with H atoms and the nearest C atoms, while the π electrons of unhydrogenated $C_{2,3,5,6}$ atoms are still delocalized and therefore contribute most to the total DOS.

To know more about the Dirac cone band structure of AB-trans C_6H_2, we plot the FSs for both the undoped case and the electron/hole doped cases. The results are shown in Fig. 6. Figure 6(a) shows that the FSs for the undoped case are two points, i.e., the two Dirac points on the Γ-M line, consistent with the band structure shown in Fig. 3(b). For the electron-doped cases, we move the Fermi level 0.1 eV, 0.2 eV, and 0.4 eV upwards, and the results are shown in Figs. 6(b), 6(c), and 6(d), respectively. It can be seen that the FSs for lightly doped cases are not circles as those in graphene but are two quasiellipses with the major axis along the Γ-M direction. With the increase of the doping level, the quasiellipses become larger. When the Fermi level moves 0.4 eV upwards, the FSs touch the boundaries of the first BZ. This implies that in an extended zone scheme, the two FSs may merge into a single FS. For the hole-doped case, we move the Fermi level -0.1 eV and -0.4 eV downwards, and the results are shown in Figs. 6(e) and 6(f), respectively. For low hole-doping levels, the FSs are also ellipselike, but at high doping levels, as seen in Fig. 6(f), the two FSs merge together and become one FS. From the above results we can obtain two conclusions. On one hand, viewed from the Dirac points, the dispersion is anisotropic along different directions. On the other hand, the dispersion shows particle-hole asymmetry for high doping levels. Combining these two results, we can conclude that AB-trans C_6H_2 is a Dirac material with anisotropic Dirac cones.

Finally, we make some further discussions. For the AB-trans C_6H_2, the lattice structure is described in Fig. 1(c). However, if one H atom forms bond with C_1 and the other H forms bond with C_2 or C_6, they are still in the form of AB-trans configuration. We check and find that the total energies for them are identical to the case in Fig. 1(c), and the electronic structures are similar to the case of the AB-trans configuration discussed above. The only difference is that the bands rotate 60° around the Γ point. For example, if the other H forms a bond with C_2, the position of the Dirac point would appear along the Γ-M' line, which rotates 60° with respect to the Γ-M line. The tilted anisotropic Dirac cone characteristic does not change, which may stimulate further experimental synthesis of the AB-trans C_6H_2. In fact, experimentally, many kinds of hydrogenated graphene systems have been realized [32,35,37,52–54]. For the periodic cases, graphane [32] and C_4H [35] were synthesized by exposing graphene in hydrogen plasma or atomic H environment. Therefore, based on these experimental developments, we hope the proposed AB-trans C_6H_2 may also be synthesised experimentally in the future.

Besides the AB-trans C_6H_2 discussed above, some other materials, such as organic compound α-$(BEDT\text{-}TTF)_2I_3$ under pressure [55–59] and half-metallic semi-Heusler alloy NiMnSb [60] also exhibit tilted anisotropic Dirac cone band structure. Furthermore, the conductance and noise for quantum transport at the Dirac point for tilted and anisotropic Dirac cones have been analyzed and studied [16]. It is found that anisotropy only affects the conductance, while a tilt Dirac cone affects both the conductance and noise. For tilted and anisotropic cones, the conductance varies strongly with transport direction; it can be either higher or lower than that of the symmetric cone. The predicted AB-trans C_6H_2 system, which shows a tilted anisotropic Dirac cone electronic

structure, provides a perfect platform to realize the above transport properties.

IV. CONCLUSION

In conclusion, we predicted a type of hydrogenated graphene, C_6H_2, and found the one in AB-trans configuration is a Dirac material with tilted anisotropic Dirac cones. The Dirac points are located on the lines from Γ to M and the Fermi surfaces are quasielliptical when doped. Around the Dirac point, the Fermi velocity varies along different directions. Accordingly, the propagation of charge carriers in this system is highly anisotropic, creating a new tunability for novel transport properties.

ACKNOWLEDGMENTS

We are thankful for helpful discussions with Nacir M. Tit. This work is supported by the Texas Center for Superconductivity at the University of Houston and the Robert A. Welch Foundation (Grant No. E-1146), the National Natural Science Foundation of China (Grants No. 11574108, No. 11104099, and No. 11204035), the Natural Science Foundation of Anhui Province in China (Grant No. 1408085QA12), and the Natural Science Research Project of Higher Education Institutions of Anhui Province in China (Grant No. KJ2015A120). The numerical calculations were performed at the Center of Advanced Computing and Data Systems at the University of Houston.

[1] O. Vafek and A. Vishwanath, Annu. Rev. Condens. Matter Phys. **5**, 83 (2014).
[2] T. O. Wehling, A. M. Black-Schaffer, and A. V. Balatsky, Adv. Phys. **63**, 1 (2014).
[3] K. S. Novoselov, A. K. Geim, S. V. Morozov, D. Jiang, Y. Zhang, S. V. Dubonos, I. V. Grigorieva, and A. A. Firsov, Science **306**, 666 (2004).
[4] A. H. Castro Neto, F. Guinea, N. M. R. Peres, K. S. Novoselov, and A. K. Geim, Rev. Mod. Phys. **81**, 109 (2009).
[5] M. Z. Hasan and C. L. Kane, Rev. Mod. Phys. **82**, 3045 (2010).
[6] X. L. Qi and S. C. Zhang, Rev. Mod. Phys. **83**, 1057 (2011).
[7] P. Richard, K. Nakayama, T. Sato, M. Neupane, Y.-M. Xu, J. H. Bowen, G. F. Chen, J. L. Luo, N. L. Wang, X. Dai, Z. Fang, H. Ding, and T. Takahashi, Phys. Rev. Lett. **104**, 137001 (2010).
[8] Z. Wang, Y. Sun, X.-Q. Chen, C. Franchini, G. Xu, H. Weng, X. Dai, and Z. Fang, Phys. Rev. B **85**, 195320 (2012).
[9] Z. Wang, H. Weng, Q. Wu, X. Dai, and Z. Fang, Phys. Rev. B **88**, 125427 (2013).
[10] Z. K. Liu, B. Zhou, Y. Zhang, Z. J. Wang, H. M. Weng, D. Prabhakaran, S.-K. Mo, Z. X. Shen, Z. Fang, X. Dai, Z. Hussain, and Y. L. Chen, Science **343**, 864 (2014).
[11] Z. K. Liu, J. Jiang, B. Zhou, Z. J. Wang, Y. Zhang, H. M. Weng, D. Prabhakaran, S-K. Mo, H. Peng, P. Dudin, T. Kim, M. Hoesch, Z. Fang, X. Dai, Z. X. Shen, D. L. Feng, Z. Hussain, and Y. L. Chen, Nat. Mater. **13**, 677 (2014).
[12] S. Borisenko, Q. Gibson, D. Evtushinsky, V. Zabolotnyy, B. Buchner, and R. J. Cava, Phys. Rev. Lett. **113**, 027603 (2014).
[13] P. Vogt, P. De Padova, C. Quaresima, J. Avila, E. Frantzeskakis, M. C. Asensio, A. Resta, B. Ealet, and G. LeLay, Phys. Rev. Lett. **108**, 155501 (2012).
[14] L. Chen, C.-C. Liu, B. Feng, X. He, P. Cheng, Z. Ding, S. Meng, Y. Yao, and K. Wu, Phys. Rev. Lett. **109**, 056804 (2012).
[15] K. I. Bolotin, K. J. Sikes, J. Hone, H. L. Stormer, and P. Kim, Phys. Rev. Lett. **101**, 096802 (2008).
[16] M. Trescher, B. Sbierski, P. W. Brouwer, and E. J. Bergholtz, Phys. Rev. B **91**, 115135 (2015).
[17] V. Pardo and W. E. Pickett, Phys. Rev. Lett. **102**, 166803 (2009).
[18] S. Banerjee, R. R. P. Singh, V. Pardo, and W. E. Pickett, Phys. Rev. Lett. **103**, 016402 (2009).
[19] J. Park, G. Lee, F. Wolff-Fabris, Y. Y. Koh, M. J. Eom, Y. K. Kim, M. A. Farhan, Y. J. Jo, C. Kim, J. H. Shim, and J. S. Kim, Phys. Rev. Lett. **107**, 126402 (2011).
[20] G. Lee, M. A. Farhan, J. S. Kim, and J. H. Shim, Phys. Rev. B **87**, 245104 (2013).
[21] Y. Feng, Z. Wang, C. Chen, Y. Shi, Z. Xie, H. Yi, A. Liang, S. He, J. He, Y. Peng, X. Liu, Y. Liu, L. Zhao, G. Liu, X. Dong, J. Zhang, C. Chen, Z. Xu, X. Dai, Z. Fang, and X. J. Zhou, Sci. Rep. **4**, 5385 (2014).
[22] W. Zhang, R. Yu, W. Feng, Y. Yao, H. Weng, X. Dai, and Z. Fang, Phys. Rev. Lett. **106**, 156808 (2011).
[23] F. Virot, R. Hayn, M. Richter, and J. van den Brink, Phys. Rev. Lett. **106**, 236806 (2011); **111**, 146803 (2013).
[24] J. Kim, S. S. Baik, S. H. Ryu, Y. Sohn, S. Park, B.-G. Park, J. Denlinger, Y. Yi, H. J. Choi, and K. S. Kim, Science **349**, 723 (2015).
[25] D. Malko, C. Neiss, F. Viñes, and A. Görling, Phys. Rev. Lett. **108**, 086804 (2012).
[26] D. Z. Yang, M. S. Si, G. P. Zhang, and D. S. Xue, Europhys. Lett. **107**, 20003 (2014).
[27] L. Z. Zhang, Z. F. Wang, Z. M. Wang, S. X. Du, H.-J. Gao, and F. Liu, J. Phys. Chem. Lett. **6**, 2959 (2015).
[28] L. C. Xu, R. Z. Wang, M. S. Miao, X. L. Wei, Y. P. Chen, H. Yan, W. M. Lau, L. M. Liu, and Y. M. Ma, Nanoscale **6**, 1113 (2014).
[29] Z. Wang, X.-F. Zhou, X. Zhang, Q. Zhu, H. Dong, M. Zhao, and A. R. Oganov, Nano Lett. **15**, 6182 (2015).
[30] C.-H. Park, L. Yang, Y.-W. Son, M. L. Cohen, and S. G. Louie, Nat. Phys. **4**, 213 (2008); Phys. Rev. Lett. **101**, 126804 (2008).
[31] S.-M. Choi, S.-H. Jhi, and Y.-W. Son, Phys. Rev. B **81**, 081407(R) (2010).
[32] D. C. Elias, R. R. Nair, T. M. G. Mohiuddin, S. V. Morozov, P. Blake, M. P. Halsall, A. C. Ferrari, D. W. Boukhvalov, M. I. Katsnelson, A. K. Geim, and K. S. Novoselov, Science **323**, 610 (2009).
[33] J. O. Sofo, A. S. Chaudhari, and G. D. Barber, Phys. Rev. B **75**, 153401 (2007).
[34] J. Zhou, Q. Wang, Q. Sun, X. S. Chen, Y. Kawazoe, and P. Jena, Nano Lett. **9**, 3867 (2009).
[35] D. Haberer, C. E. Giusca, Y. Wang, H. Sachdev, A. V. Fedorov, M. Farjam, S. A. Jafari, D. V. Vyalikh, D. Usachov, X. Liu, U. Treske, M. Grobosch, O. Vilkov, V. K. Adamchuk, S. Irle, S. R. P. Silva, M. Knupfer, B. Büchner, and A. Grüneis, Adv. Mater. **23**, 4497 (2011).
[36] L. Feng and W. X. Zhang, AIP Adv. **2**, 042138 (2012).

[37] R. Balog, B. Jørgensen, L. Nilsson, M. Andersen, E. Rienks, M. Bianchi, M. Fanetti, E. Lægsgaard, A. Baraldi, S. Lizzit, Z. Sljivancanin, F. Besenbacher, B. Hammer, T. G. Pedersen, P. Hofmann, and L. Hornekær, Nat. Mater. **9**, 315 (2010).
[38] P. Chandrachud, B. S. Pujari, S. Haldar, B. Sanyal, and D. G. Kanhere, J. Phys.: Condens. Matter **22**, 465502 (2010).
[39] M. Yang, A. Nurbawono, C. Zhang, Y. P. Feng, and Ariando, Appl. Phys. Lett. **96**, 193115 (2010).
[40] H. Gao, L. Wang, J. Zhao, F. Ding, and J. Lu, J. Phys. Chem. C **115**, 3236 (2011).
[41] H.-C. Huang, S.-Y. Lin, C.-L. Wu, and M.-F. Lin, Carbon **103**, 84 (2016).
[42] P. O. Lehtinen, A. S. Foster, Yuchen Ma, A. V. Krasheninnikov, and R. M. Nieminen, Phys. Rev. Lett. **93**, 187202 (2004).
[43] S. Casolo, O. M. Løvvik, R. Martinazzo, and G. F. Tantardini, J. Chem. Phys. **130**, 054704 (2009).
[44] E. J. Duplock, M. Scheffler, and P. J. D. Lindan, Phys. Rev. Lett. **92**, 225502 (2004).
[45] B. S. Pujari, S. Gusarov, M. Brett, and A. Kovalenko, Phys. Rev. B **84**, 041402(R) (2011).
[46] D. W. Boukhvalov, M. I. Katsnelson, and A. I. Lichtenstein, Phys. Rev. B **77**, 035427 (2008).
[47] H.-Y. Lu, L. Hao, R. Wang, and C. S. Ting, Phys. Rev. B **93**, 241410(R) (2016).
[48] P. Giannozzi, S. Baroni, N. Bonini, M. Calandra, R. Car, C. Cavazzoni, D. Ceresoli, G. L. Chiarotti, M. Cococcioni, I. Dabo, A. D. Corso, S. de Gironcoli, S. Fabris, G. Fratesi, R. Gebauer, U. Gerstmann, C. Gougoussis, A. Kokalj, M. Lazzeri, L. Martin-Samos, N. Marzari, F. Mauri, R. Mazzarello, S. Paolini, A. Pasquarello, L. Paulatto, C. Sbraccia, S. Scandolo, G. Sclauzero, A. P. Seitsonen, A. Smogunov, P. Umari, and R. M Wentzcovitch, J. Phys.: Condens. Matter **21**, 395502 (2009); http://www.quantum-espresso.org.
[49] G. Kresse and D. Joubert, Phys. Rev. B **59**, 1758 (1999).
[50] J. P. Perdew, K. Burke, and M. Ernzerhof, Phys. Rev. Lett. **77**, 3865 (1996).
[51] S. Baroni, S. de Gironcoli, and A. D. Corso, Rev. Mod. Phys. **73**, 515 (2001).
[52] R. Balog, B. Jørgensen, J. Wells, E. Lægsgaard, P. Hofmann, F. Besenbacher, and L. Hornekær, J. Am. Chem. Soc. **131**, 8744 (2009).
[53] W.-K. Lee, K. E. Whitener. Jr., J. T. Robinson, and P. E. Sheehan, Adv. Mater. **27**, 1774 (2015).
[54] H. Sahin, O. Leenaerts, S. K. Singh, and F. M. Peeters, Wiley Interdiscip. Rev.: Comput. Mol. Sci. **5**, 255 (2015).
[55] M. O. Goerbig, J.-N. Fuchs, G. Montambaux, and F. Piéchon, Phys. Rev. B **78**, 045415 (2008).
[56] A. Kobayashi, S. Katayama, K. Noguchi, and Y. Suzumura, J. Phys. Soc. Jpn. **73**, 3135 (2004).
[57] S. Katayama, A. Kobayashi, and Y. Suzumura, J. Phys. Soc. Jpn. **75**, 054705 (2006).
[58] H. Kino and T. Miyazaki, J. Phys. Soc. Jpn. **75**, 034704 (2006).
[59] T. Morinari, T. Himura, and T. Tohyama, J. Phys. Soc. Jpn. **78**, 023704 (2009).
[60] S. J. Jenkins, Phys. Rev. B **82**, 020403(R) (2010).